Available online at www.sciencedirect.com
ScienceDirect
Ceramics International 34 (2008) 1975–1981
CERAMICS INTERNATIONAL
www.elsevier.com/locate/ceramint

Microstructure and non-isothermal oxidation mechanism of biomorphic carbon template

Pengzhao Gao *, Yongmei Bai, Sen Lin, Weiming Guo, Hanning Xiao

College of Materials Science and Engineering, Hunan University, Changsha 410082, PR China

Received 20 December 2006; received in revised form 25 April 2007; accepted 18 July 2007
Available online 19 August 2007

Abstract

A biomorphic carbon template (BCT) was prepared by carbonizing pine wood under Ar atmosphere. Microstructure and component of BCT were performed by scanning electron microscopy (SEM), energy dispersive X-ray spectroscopy (EDS) and X-ray diffraction (XRD). The pyrolytic behavior of pine wood converse to carbon template and non-isothermal oxidation properties of BCT were studied by thermogravimetric analysis (TGA). Experimental results show that BCT has a topologically uniform interconnected porous network microstructure, and is typical non-graphitizable carbon. With increasing carbonization temperature, the (0 0 2) peak becomes stronger, the interplanar spacing decrease, the structure of BCT slowly evolved toward that of ideal graphite. The oxidation reaction of BCT begins at 406.5 °C, and the reaction rate reaches maximum when the residual weight is 36.9%. The oxidation mechanism is one-dimensional diffusion, the kinetic parameters are: lg A (min^{-1}) = 10.367 and E_α (kJ mol^{-1}) = 164.17.

Keywords: Precursors: organic; X-ray methods; Chemical properties; Carbon

1. Introduction

Biomorphic templet is a new concept for fabricating ceramic materials with novel hierarchical and complex microstructures using natural biological materials as templates, such as wood [1], rattan [2], rice husk [3].

Amongst these, wood has been paid considerable attention with respect to the conversion of its tissue to ceramic materials because it has highly anisotropic cellular structures [4]. Wood has been used to fabricate various novel ceramics with micro-, meso- and macro-structures, classified into the following two groups according to the density or porosity of the products.

Initially, ceramic materials derived from wood were mainly dense or low-porosity SiC, SiC/Si or oxide ceramic composites prepared by the infiltration of silicon melt or oxide precursors into charcoals [5–7]. These materials usually possess high mechanical performances, but do not effectively utilize the pore microstructure of wood. Now, more attention is focused on fabricating porous ceramics from wood. For example, porous biomorphic oxide ceramics such as Al_2O_3 [8], and TiO_2 [9] are prepared via the combination of the infiltration of metal alkoxide or oxide sols into charcoal and subsequent oxidation in air at high temperatures. Wood-derived cellular ceramics might be of interest for high-temperature-resistant exhaust gas filters, catalyst carriers, advanced microreactor systems, immobilization supports for living cells, microbes or enzymes, and waste water treatment, as well as acoustic and heat insulation structures, etc.

For the wood-derived cellular ceramics, the microstructure and thermal oxidation properties of porous carbon template make an important influence on the structure and performance of products. However, little work has been done on the study of microstructure and thermal oxidation properties of BCT systemically.

TGA methods (thermogravimetry, differential thermogravimetry) are widely used in the process of studying the oxidation mechanism of carbon materials [10,11]. The results can supply very useful information on the processes of oxidation decomposition of these kinds of materials and their thermal oxidation stability.

In the present work, the biomorphic carbon template is derived from pine wood under Ar atmosphere. The effects of

* Corresponding author. Tel.: +86 731 8822269.
E-mail address: gaopengzhao7602@hnu.cn (P. Gao).

0272-8842/$34.00
doi:10.1016/j.ceramint.2007.07.025

carbonization temperature on the microstructure and basic properties of resulted biomorphic template are investigated in detail. The non-isothermal oxidation mechanism of BCT is studied systemically.

2. Experimental

2.1. Material preparation

Pine wood was purchased from Changsha Wood Co. (Changsha, PR China). Wood was shaped, dried at 120 °C for 48 h, and subsequently carbonized under Ar atmosphere with a flow rate of 50 ml min^{-1} at 800, 1200, 1500, 1700 °C for 4 h in a graphite heater furnace, resulting in a porous biomorphic carbon template (BCT). The heating process was determined through the study of pyrolytic behavior of pine wood.

2.2. Characterization of BCT

The morphology and quantitative elemental analyses of the BCT were characterized by scanning electron microscopy (SEM, JEOL, JSM-6700F)) equipped with an energy dispersive spectrometry (EDS, Oxford).

The extent of carbonization was estimated from X-ray diffraction (XRD, D5000, Siemens). An X-ray Diffractometer using nickel filtered Cu K_α radiation produced at 30 kV and 30 mA. Scanning speeds were 2° min^{-1} for recording of all possible profiles and for calculations of XRD parameters, respectively. From the position of the (0 0 2) peak ($2\theta_{(002)}$) in X-ray diffractogram, the $d_{(002)}$ interplanar spacing was determined using the Bragg equation:

$$d_{(002)} = \frac{\lambda}{2\sin\theta_{(002)}} \quad (1)$$

The pyrolytic behavior of pine wood was characterized using thermogravimetric analysis (TGA) and differential scanning calorimetry (DSC) in a Ar flow rate of 50 ml min^{-1} 1 with a heating rate of 10 °C min^{-1} from room temperature to 800 °C. The initial mass of sample was about 7.0 mg.

TGA was performed on thermal analyzer (model Netzsch Thermische Analyzer, STA 409C) with alumina powder as the reference sample.

The oxidation properties and mechanism of BCT were measured using the same thermal analyzer under the same conditions only in air atmosphere.

3. Results and discussion

3.1. Pyrolytic conversion of wood to carbon template

Wood may be converted into a carbon template that retains the anatomical features of wood by controlled thermal decomposition process. In order to study the decomposition behavior of wood, some small pieces were heated in the thermal analyzer in Ar atmosphere. As is known, the three major components of wood, namely hemicellulose, cellulose and lignin, break down in a stepwise manner [12,13].

Fig. 1 shows the TG-DTG curves of dried pine wood at a temperature range of 25–800 °C. It can be seen that weight-loss of wood proceeds in two stages. The first weight-loss stage starts at 30 °C, reaches a maximum rate at 56.7 °C, the weight-loss is about 4%, which may be the removal of moisture.

The second weight-loss process starts at 200 °C, reaches a maximum rate at 367.5 °C and it is almost terminated at 500 °C, minimal weight-loss occurs afterward [6], the weight-loss in this stage is about 74%. During the second step of weight-loss, the decomposition of hemicellulose takes place at around 190–280 °C and volatile products are released (CO_2, CO, and other organics vapors). In the temperature range of 280–500 °C, major weight-loss takes place due to the decomposition of cellulose and lignin. The decomposition of lignin increases above 300 °C and results in a rapid increase in carbon content of the material.

Above 800 °C, thermal induced decomposition and rearrangement reactions are almost terminated leaving a carbon template structure [14].

From Fig. 1, it can be seen that between 200 and 500 °C, almost 80% of the total weight-loss occurs due to evolution of H_2O, CO_2, and volatile hydrocarbon species from decomposition reactions via the open pore channel system of wood. The carbon template is shown to be easily machined to net shape prior to conversion to a ceramic material. Thus, in order to retain the anatomical features of wood, the prolyitc process of pine wood used in this experiment was a slow heating rate of 2 °C min^{-1} up to 600 °C and a higher rate of 5 °C min^{-1} up to the aim temperature.

3.2. The effects of temperature on carbonization extent of bimorphic carbon template

Fig. 2 shows the XRD patterns of BCT obtained from pine wood by carbonizing at various temperatures. The two broad diffraction bands are observed in Fig. 2, indicating that the BCT is amorphous.

For carbon template obtained at 800 °C, it can be seen that there are two main analogous graphitic peaks corresponding to

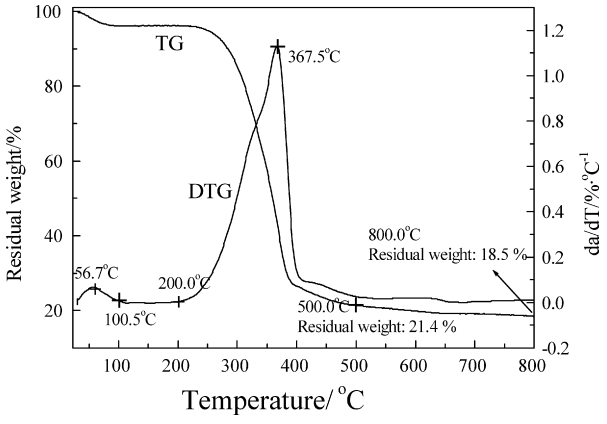

Fig. 1. TG-DTG curves of pine wood in Ar atmosphere.

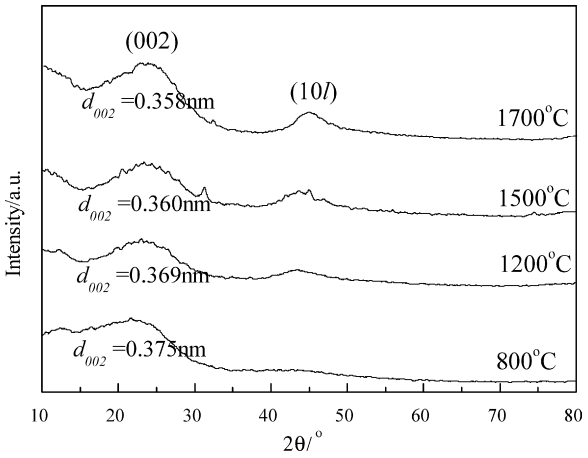

Fig. 2. The XRD patterns of BCT treated in different temperature.

a broad (0 0 2) peak and a lower intensity (10 *l*) peak. This is suggestive of the development of hexagonal network layers stacked roughly parallel to each other, i.e. turbostratic structure [15], which indicates the regularity of carbon in BCT is poor.

Judging from the weak intensity and broadness, the peak (0 0 2) profile of carbon template consists of three components that correspond to amorphous (B), turbostratic (T) and graphite (G) components. With the increase of carbonization temperature, the T and G components increase and B component decreases [16].

From Fig. 2, it can also be seen that the (0 0 2) peak becomes stronger, shifts to larger 2θ angles, and it has a smaller full-width at half-maximum intensity with increasing carbonization temperature from 800 to 1700 °C. The results is as expected for non-graphitizable carbonized cellulose [15], which means that the T and G components became larger. This implies that the regularity of the carbons in carbon template became better; consequently their structure became more rigid and stable.

The narrowing of (0 0 2) peak is indicative of developing atomic order in BCT. It is noted that the profile of (10 *l*) peak changes from a symmetric one below 1500 °C to asymmetrical for 1700 °C, revealing the turbostratic nature of BCT. However, it seems that three-dimensional crystallinity is almost not developed even after carbonization at 1700 °C because the (0 0 4) peak and the splitting of (10 *l*) peak to (1 0 0) and (1 0 1) peaks can hardly be observed.

The d(0 0 2) value is traditionally used to estimate a graphitization degree of carbon. In general, growing disorder in the materials is reflected in increased values of $d_{(002)}$ [17]. As shown in Fig. 2, the (0 0 2) interplanar spacing of the crystalline decreases with increasing carbonization temperature, which means the structure of BCT slowly evolved toward that of ideal graphite. Crystalline graphite exhibits a sharp peak and an

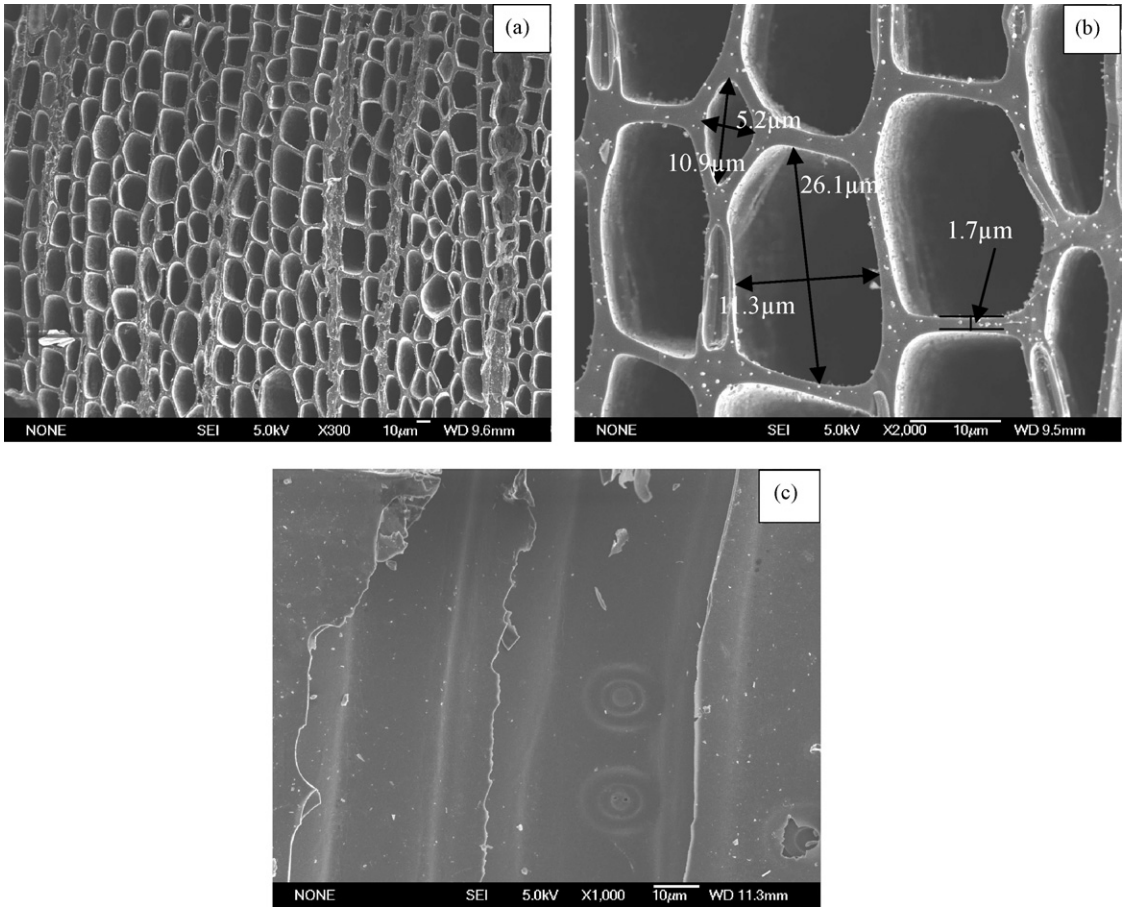

Fig. 3. SEM micrographs of (a and b) cross-section perpendicular to axial direction and (c) cross-section parallel to axial direction of biomorphic carbon template.

interplanar spacing close to 0.3354 nm [18]. All $d_{(002)}$ values of BCT are much higher than that of ideal graphite, indicating the non-graphitizable characteristics of BCT. These results suggest that BCT carbonized at experimental temperatures is not composed of a completely graphitized carbon, but has a turbostratic structure [19,20]. The graphene layers became more extended, their spacing closer, and the graphene stacks higher with increasing carbonization temperature [21].

3.3. Microstructure characterization of bimorphic carbon template

Fig. 3 shows the SEM micrographs of BCT (carbonization at 1200 °C). As seen in Fig. 3, the microstructure of BCT shows hollow channels of various diameters that originate from tracheid cells are parallel to the axis of the tree (as shown in Fig. 3c). Hollow channels of biocarbon template have uniform arrangement, where the black part is lumen and grey part is carbon layer formed by carbonization of cell wall (as shown in Fig. 3a and b). The difference in diameters of hollow channels is attributed to the non-uniform distribution of texture of wood. The average range of the diameters of cells is about 5–30 μm, and cell wall (thickness of carbon layer) is about 2–3 μm. Most of the cellular pores show a rectangular shape and the distribution shows regular net with carbon wall joint each other. The cell topologically uniform arrangement of early wood is interrupted by growth ring patterns, where late wood cells show a significantly higher strut thickness.

Fig. 4 displays the EDS spectrum of BCT measured with the same system. The peaks at 0.28 and 0.52 keV are from carbon and manganese, respectively, the peak at 3.70 keV is due to calcium in the sample. The ratio of C:Mn:Ca are 99.04:0.83:0.13 in atom amounts. The Ca and Mn may be the inorganic salt absorbed in wood growth process.

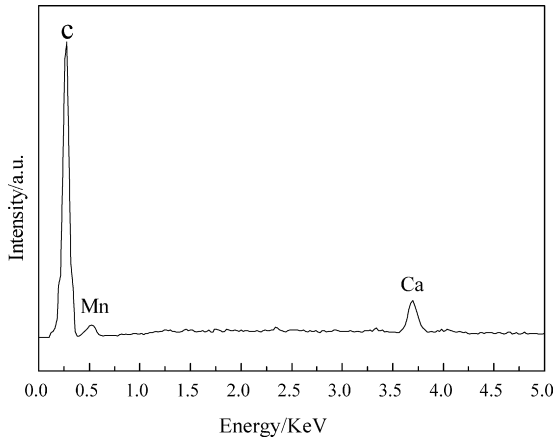

Fig. 4. EDS spectrum of BCT.

3.4. Thermal oxidation stability study

Fig. 5 shows the TG-DTG curves of BCT (carbonization at 1200 °C) in Ar and air at 10 °C min^{-1}. It can be seen that the weight-loss of BCT proceeds in two stages in the temperature range of 30–400 °C. In the first stage from room temperature to 100 °C, the mass loss is about 4–6%, which is attributed to the loss of physically adsorbed water. The second stage lasts in a temperature range of 100–400 °C. In this stage, the mass loss is 2–8%, which is attributed to the loss of physically adsorbed gaseous CO_2. This is in conformity with the cases reported on coal. Above 400 °C, the weight-loss is slight in Ar, but rapidly increase in air, which shows the BCT starts oxidizing.

From the TG curve of BCT in air, it is obvious that the material is oxidized from 406.5 °C and it is burnt out at 582.6 °C. The oxidation weight-loss increases with the increasing of temperature. From the DTG curve, it is easy to see that the oxidation rate (da/dT) of BCT increases firstly and then decreases with the increasing of temperature. Combined with TG and DTG curves, it can be clearly seen that the oxidation rate increases firstly and then decreases with the increasing of weight-loss; it reaches a maximum when the residual weight is 36.9%.

3.5. Study of oxidation kinetics and mechanism of bimorphic carbon template

Non-isothermal TGA is a powerful tool to calculate the activity energy and determine the mechanism function of an oxidation decomposition reaction for solid materials. The

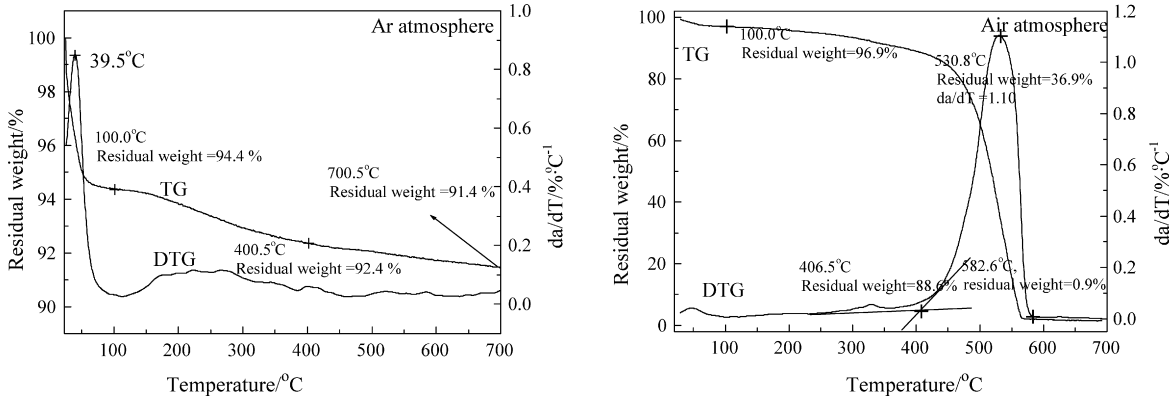

Fig. 5. The TG-DTG curves of BCT in Ar and air atmosphere.

Table 1
Oxidation decomposition data of BCT from TG and DTG curves

T (K)	a	da/dT (%K^{-1})	T (K)	a	da/dT (%K^{-1})	T (K)	a	da/dT (%K^{-1})
380.5	0.10	0.046	507.4	0.40	0.872	536.4	0.70	1.075
445.9	0.15	0.154	512.9	0.45	0.964	541.3	0.75	1.049
469.1	0.20	0.312	518.0	0.50	1.027	545.7	0.80	1.012
483.1	0.25	0.457	522.8	0.55	1.064	550.9	0.85	0.946
493.2	0.30	0.591	527.3	0.60	1.082	556.1	0.90	0.821
501.2	0.35	0.747	532	0.65	1.085	561.5	0.95	0.596

Table 2
Mechanism function of thermal decomposition kinetic equation

Name of function	Type of mechanism		Form of function		No
			$F(a)$	$G(a)$	
Avrami-Erofeev equation	Random nucleation	$n = 1$	$(1 - a)$	$-\ln(1 - a)$	A1
		$n = 2$	$2(1 - a)[-\ln(1 - a)]^{1/2}$	$[-\ln(1 - a)]^{1/2}$	A2
		$n = 3$	$3(1 - a)[-\ln(1 - a)]^{2/3}$	$[-\ln(1 - a)]^{1/3}$	A3
Parabola law	1-D diffusion, decelerator a–t curve		$1/(2a)$	a^2	D1
Valensi equation	2-D diffusion, decelerator a–t curve		$[-\ln(1 - a)]^{-1}$	$a + (1 - a)\ln(1 - a)$	D2
Jander equation	3-D diffusion, decelerator a–t curve		$1.5(1 - a)^{2/3}[1 - (1 - a)^{1/3}]^{-1}$	$[1 - (1 - a)^{1/3}]^2$	D3
Anti-Jander equation	3-D diffusion		$1.5(1 + a)^{2/3}[(1 + a)^{1/3} - 1]^{-1}$	$[(1 + a)^{1/3} - 1]^2$	D4
G.-B. equation*	3-D diffusion, spherical symmetry		$1.5\ [(1 - a)^{-1/3} - 1]^{-1}$	$[1 - 2a/3] - (1 - a)^{2/3}$	D5
Z.-L.-T equation**	3-D diffusion		$1.5(1 - a)^{4/3}[(1 - a)^{-1/3} - 1]^{-1}$	$[(1 - a)^{-1/3} - 1]^2$	D6
Chemical reaction	$n = 2$ decelerator a–t curve		$(1 - a)^2$	$(1 - a)^{-1}$	F2
Reaction order	$n = 2$		$0.5(1 - a)^{-1}$	$1 - (1 - a)^2$	R2
	$n = 3$		$1/3(1 - a)^{-2}$	$1 - (1 - a)^3$	R3

* Ginstling-Brounstein equation.
** Zhuralev-Lesokin-Tempelman equation.

Table 3
Kinetic parameters obtained from different treatment methods

No.	Achar-Brindly-Sharp				Satava-Sestak			
	E_α (kJ mol^{-1})	lg A (min^{-1})	r	S.D.	E_α (kJ mol^{-1})	lg A (min^{-1})	r	S.D.
A1	186.10	13.63	−0.980	0.215	123.30	7.418	−0.980	0.075
A2	121.30	9.10	−0.980	0.152	61.60	3.492	−0.980	0.037
A3	99.70	7.52	−0.978	0.140	41.10	2.259	−0.980	0.025
D1	**166.70**	**11.89**	**−0.992**	**0.260**	**165.10**	**9.692**	**−0.995**	**0.047**
D2	209.50	14.62	−0.996	0.125	186.50	10.940	−0.994	0.063
D3	263.80	17.78	−0.996	0.162	215.00	12.342	−0.988	0.099
D4	228.40	15.29	−0.998	0.086	195.70	10.949	−0.992	0.073
D5	228.40	15.29	−0.998	0.086	195.90	10.966	−0.992	0.072
D6	370.10	25.25	−0.972	0.586	282.40	17.211	−0.968	0.216
F2	292.40	21.10	−0.948	0.640	101.00	6.522	−0.843	0.192
R2	133.00	9.60	−0.995	0.090	100.50	5.521	−0.991	0.039
R3	150.70	10.66	−0.995	0.096	107.60	5.837	−0.988	0.049

No.	Coats-Redfern				No.				
	E_α (kJ mol^{-1})	lg A (min^{-1})	r	S.D.		E_α (kJ mol^{-1})	lg A (min^{-1})	r	S.D.
A1	116.70	6.950	−0.976	0.170	D4	192.80	10.901	−0.991	0.166
A2	51.90	2.371	−0.970	0.084	D5	193.10	10.919	−0.992	0.165
A3	30.30	0.728	−0.963	0.055	D6	284.10	17.490	−0.966	0.496
D1	**160.70**	**9.490**	**−0.995**	**0.108**	F2	93.30	5.870	−0.810	0.440
D2	183.20	10.849	−0.993	0.142	R2	92.80	4.866	−0.989	0.089
D3	213.20	12.378	−0.987	0.226	R3	100.20	5.244	−0.986	0.111

results can explain the oxidation process. In the present work, the equations of Achar-Brindley-Sharp-Wendworth, Satava-Sestak and Coats-Redfern [10] were used to study the oxidation mechanism of BCT.

Achar-Brindley-Sharp-Wendworth equation:

$$\ln\left[\frac{1}{F(a)}\frac{\mathrm{d}a}{\mathrm{d}T}\right] = \ln\left(\frac{A}{\beta}\right) - \frac{E_\alpha}{R}\frac{1}{T} \quad (2)$$

Satava-Sestak equation:

$$\lg[G(a)] = \lg\left(\frac{AE_\alpha}{\beta R}\right) - 2.135 - \frac{0.4567E_\alpha}{R}\frac{1}{T} \quad (3)$$

Coats-Redfern equation:

$$\ln\frac{G(a)}{T^2} = \ln\left(\frac{AR}{\beta E_\alpha}\right) - \frac{E_\alpha}{R}\frac{1}{T} \quad (4)$$

where A is pre-exponential factor, β the heating rate, α the concersion, T the absolute temperature in K, E_α the activation energy in kJ mol^{-1}, R the gas constant in J mol^{-1} K^{-1}, $F(a)$ and $G(a)$ the differential and integral mechanism function, respectively.

The basic data of a, T and da/dT obtained by the TG-DTG curves are listed in Table 1.

The integral ($G(a)$) and differential ($F(a)$) functions for the most common mechanisms used in kinetic study of solid-state decomposition in this work are listed in Table 2 [10,22].

The kinetic analyses are completed by the linear least-squares method on a computer. According to Eqs. (2)–(4), the values of linear correlation coefficient r and standard deviation S.D. are obtained from ln[(da/dT)/$F(a)$], log[$G(a)$] and ln[$G(a)$/T^2] versus $1/T$ lines directly, the values of E_α and A can be calculated from the slope and intercept of above lines, respectively. The results (E_α, A, r and S.D.) of ln[(da/dT)/$F(a)$], log[$G(a)$], ln[$G(a)/T^2$] versus $1/T$ for all possible mechanisms ($F(a)$ *and* $G(a)$) are listed in Table 3.

If the following conditions:

(1) The values of E_α were between 80 and 250 kJ mol^{-1} and the values of lg A were between 7 and 30 min^{-1}, which were obtained by the different methods were approximately equal;
(2) The linear relevant coefficient r was better (<-0.98);
(3) The standard deviation S.D. was small (<0.3).were all satisfied at the same time. It can be concluded that the relevant function was the probable mechanism of oxidation reaction [23,24].

From the data in Table 3, it can be seen clearly that only function D1 (bold values in Table 3) satisfied the above-mentioned conditions. Thus, the possible mechanism function was function D1 (D1 stood for 1-D diffusion, decelerator a–t curve). We conclude that the kinetic equation for the oxidation reaction of BCT was $\mathrm{d}a/\mathrm{d}T = (A/\beta)\exp(-E_a/RT)(0.5a^{-1})$. The kinetic parameters are: lg A (min^{-1}) = 10.367 and E_α (kJ mol^{-1}) = 164.17.

4. Conclusions

In the present study, a biomorphic carbon template made from pine wood was developed. The basic structure characterization and oxidation kinetics of BCT were investigated. The results are summarized as follows:

(1) The biomorphic carbon template has a topologically uniform interconnected porous network microstructure, and is typical non-graphitizable carbon. With increasing carbonization temperature, the (0 0 2) peak becomes stronger, the (0 0 2) interplanar spacing decrease, the structure slowly evolved toward that of ideal graphite.
(2) BCT was oxidized from 406.5 °C and the oxidation rate increases firstly and then decreases with the increasing of weight-loss, it reaches a maximum when the residual weight is 36.9%.
(3) The oxidation mechanism was one-dimensional diffusion. The kinetic parameters are: lg A (min^{-1}) = 10.367 and E_α (kJ mol^{-1}) = 164.17.

References

[1] C.R. Rambo, J. Cao, O. Rusina, H. Sieber, Manufacturing of biomorphic (Si, Ti, Zr)-carbide ceramics by sol–gel processing, Carbon 43 (2005) 1174–1183.
[2] A. Zampieri, S. Kullmann, T. Selvam, J. Bauer, W. Schwieger, H. Sieber, T. Fey, P. Greil, Bioinspired rattan-derived SiSiC/Zeolite monoliths: preparation and characterisation, Micropor. Mesopor. Mater. 90 (1–3) (2006) 162–174.
[3] V. Martínez, M.F. Valencia, J. Cruz, J.M. Mejía, F. Chejne, Production of β-SiC by pyrolysis of rice husk in gas furnaces, Ceram. Int. 32 (8) (2006) 891–897.
[4] C. Zollfrank, R. Kladny, H. Sieber, Biomorphous SiOC/C ceramic composites from chemically modified wood templates, J. Eur. Ceram. Soc. 24 (2004) 479–487.
[5] A. Hofenauer, O. Treusch, F. Tröger, Dense reaction infiltrated silicon/silicon carbide ceramics derived from wood based composites, Adv. Eng. Mater. 5 (11) (2003) 794–799.
[6] M. Singh, J.A. Salem, Mechanical properties and microstructure of biomorphic silicon carbide ceramics fabricated from wood precursors, J. Eur. Ceram. Soc. 22 (14/15) (2002) 2709–2717.
[7] M. Singh, B.M. Yee, Reactive processing of environmentally conscious, biomorphic ceramics from natural wood precursors, J. Eur. Ceram. Soc. 24 (2004) 209–217.
[8] M. Mizutani, H. Takase, N. Adachi, T. Ota, K. Daimon, Y. Hikichi, Porous ceramics prepared by mimicking silicified wood, Sci. Technol. Adv. Mater. 6 (1) (2005) 76–83.
[9] B.H. Sun, T.X. Fan, D. Zhang, Porous TiC ceramics derived from wood template, J. Porous Mat. 9 (4) (2002) 275–277.
[10] Gao Pengzhao, Xiao Hanning, Wang Hongjie, Jin Zhihao, A study on the oxidation kinetics and mechanism of three-dimensional (3D) carbon fiber braid coated by gradient SiC, Mat. Chem. Phys. 93 (2005) 164–169.
[11] Pengzhao Gao, Weiming Guo, Hanning Xiao, Guo Jun, Model-free kinetics applied to the oxidation properties and mechanism of three-dimension carbon/carbon composite, Mater. Sci. Eng. A 432 (1–2) (2006) 226–230.
[12] P. Ehrburger, L. Lahaye, E. Wozniak, Effect of carbonization on the porosity of beechwood, Carbon 20 (5) (1982) 433–439.
[13] C.E. Byrne, D.C. Nagle, Carbonization of wood for advanced materials applications, Carbon 35 (2) (1997) 259–266.
[14] P. Greil, Biomorphous ceramics from lignocellulosics, J. Eur. Ceram. Soc. 21 (2) (2001) 105–118.
[15] A. Onodera, K. Terashima, T. Urushihara, High-pressure synthesis of diamond from phenolic resin, J Mater Sci 32 (1997) 4309–4318.

[16] H.M. Cheng, H. Endo, T. Okabe, Graphitization behavior of wood ceramics and bamboo ceramics as determined by X-ray diffraction, J. Porous Mater. 6 (3) (1999) 233–237.
[17] A. Cuesta, P. Dhamelincourt, J. Laureyns, Comparative performance of X-ray diffraction and Raman microprobe techniques for the study of carbon materials, J. Mater. Chem. 8 (12) (1998) 2875–2879.
[18] M. Shiraishi, New Introduction to Carbon Materials, Realize, Tokyo, 1996pp.24–31.
[19] A. Braun, M. Bärtsch, B. Schnyder, X-ray scattering and adsorption studies of thermally oxidized glassy carbon, J. Non-cryst. Solids 260 (1999) 1–14.
[20] T. Hirose, T.X. Fan, T. Okabe, Effect of carbonization temperature on the basic properties of woodceramics impregnated with liquefied wood, J. Mater. Sci. 36 (17) (2001) 4145–4149.
[21] A. Braun, M. Bärtsch, B. Schnyder, R. Kötz, O. Haas, H.G. Haubold, G. Goerigk, X-ray scattering and adsorption studies of thermally oxidized glassy carbon, J. Non-Cryst. Solids 260 (1–2) (1999) 1–14.
[22] M.A. Gabal, Kinetics of the thermal decomposition of CuC_2O_4–ZnC_2O_4 mixture in air, Thermochim. Acta 402 (1–3) (2003) 199–208.
[23] Tonglai Zhang, Rongzu Hu, Fuping Li, A method to determine the non-isothermal kinetic parameters and select the most probable mechanism function using a single non-isothermal DSC curve, Thermochem. Acta 244 (1994) 177–184.
[24] Rongzu Hu, Zhengquan Yang, Yanjun Liang, The determination of the most probable mechanism function and three kinetic parameters of exothermic decomposition reaction of energetic materials by a, Thermochem. Acta 123 (1988) 135–151.